

# Quasinormal modes in semi-open systems

Leonardo Solidoro,<sup>1,2,\*</sup> Sam Patrick,<sup>3</sup> Ruth Gregory,<sup>3,4</sup> and Silke Weinfurter<sup>1,2,5</sup>

<sup>1</sup>*School of Mathematical Sciences, University of Nottingham, University Park, Nottingham, NG7 2RD, UK*

<sup>2</sup>*Nottingham Centre of Gravity, University of Nottingham, University Park, Nottingham NG7 2RD, UK*

<sup>3</sup>*Department of Physics, King's College London, University of London, Strand, London, WC2R 2LS, UK*

<sup>4</sup>*Perimeter Institute, 31 Caroline Street North, Waterloo, ON, N2L 2Y5, Canada*

<sup>5</sup>*Centre for the Mathematics and Theoretical Physics of Quantum*

*Non-Equilibrium Systems, University of Nottingham, Nottingham, NG7 2RD, UK*

(Dated: July 1, 2024)

Astrophysical black holes are open systems which, when perturbed, radiate quasi-normal modes (QNMs) to infinity. By contrast, laboratory analogues are necessarily finite-sized, presenting a potential obstacle to exciting QNMs in the lab. In this study, we investigate how the QNM spectrum of a toy-model black hole is modified when the system is enclosed by a partially reflecting wall. Counter to expectation, we demonstrate that QNMs not only persist in finite-sized systems, but the number of detectable modes increases. Furthermore, we show that QNMs in this set-up can be easily excited by incoherent background noise. Our findings align with studies exploring the spectral stability of black holes, such as those examining small modifications of the surrounding gravitational field. Importantly, our work paves the way for exploring spectral stability in laboratory systems, enabling experimental investigation of black hole features in closed systems.

*Introduction.*—The success of the black hole spectroscopy program is founded on the use of gravitational waves produced by merging binaries as a probe of the system's properties [1]. At late times during the so-called *ringdown* phase, the remnant emits a characteristic signal as it sheds energy and relaxes into its final state. This signal consists of a discrete set of damped harmonic oscillators referred to as quasinormal modes (QNMs) [2–6], which are natural resonances of linear open systems. Next generation gravitational wave detectors such as LISA and Einstein telescope will profit from enhanced sensitivity [7, 8], making it paramount to understand how the ringdown is influenced by various high-order effects, e.g. environmental factors [9] and nonlinearities [10].

Recent investigation into the spectral stability of black holes has demonstrated the susceptibility of the QNM spectrum to small, local perturbations to the scattering potential experienced by gravitational waves around a black hole [11–14]. In some cases, the spectrum can even admit additional long-lived modes called quasi-bound states, potentially leading to higher-order effects as a result of their long lifetimes [15, 16]. Understanding such modifications of the QNM spectrum may have important consequences for the black hole spectroscopy programme [17, 18]. In this regard, it is natural to consider non-perturbative scenarios where energy is retained by the system due to an effective reflection mechanism acting on escaping radiation. Such situations arise naturally in gravity in the context of neutron stars [4], exotic compact objects [19–22] and asymptotically anti-de Sitter spacetimes [6].

Gravity simulators present an ideal platform where such an enquiry can be pursued. These are physical sys-

tems in which excitations behave as though they propagate on a curved spacetime, permitting the experimental investigation of elusive phenomena like Hawking radiation [23–26] and rotational superradiance [27–31]. Notably, ringdown signals have been studied in polariton superfluids [32], optical solitons [33] and in hydrodynamic systems [34, 35]. Although treating these platforms as effectively open systems is usually justified by a combination of energy dissipation, limited temporal evolution and engineering of absorptive boundaries, a complete analysis should not neglect finite-size effects resulting from confinement mechanisms. This is particularly true of our recent superfluid helium gravity simulator [36], where dissipation is strongly reduced and many reflections from the container wall can occur during the experimental time-frame.

All of this serves to emphasise the importance of understanding how finite-size effects modify the QNM spectrum in the context of both black hole physics and gravity simulators. In this Letter, we study the effect of a partially reflective boundary on the QNM spectrum of the Pöschl-Teller (PT) potential, a model which appears in both black hole physics [2, 6] and analogue systems [33, 37], demonstrating how finite-size effects endow the system with an additional control parameter that can be exploited in the experimental study of QNMs.

*General set-up.*—A simple system which captures the essential physics of QNMs is the one-dimensional wave equation with a repulsive potential  $V(x)$  [4, 6],

$$\left(\frac{\partial^2}{\partial t^2} - \frac{\partial^2}{\partial x^2} + V(x)\right)\Psi = 0, \quad (1)$$

where the wave speed is set to unity and we assume  $V \rightarrow 0$  as  $x \rightarrow \pm\infty$ . QNMs are resonances of open systems, i.e. systems that lose energy, in this case, to spatial infinity. By looking for solutions of the form  $\Psi(x, t) = e^{-i\omega t}\psi(x)$ , the wave equation reduces to a

\* leonardo.solidoro@nottingham.ac.uk

Schrödinger-like equation  $\psi'' + [\omega^2 - V(x)]\psi = 0$ , and the set of QNMs are found as the set of frequencies whose related modes satisfy the purely out-going boundary conditions,

$$\lim_{x \rightarrow \pm\infty} \psi \propto e^{\pm i\omega x}. \quad (2)$$

More generally, the problem of calculating QNMs can be formulated as a scattering problem. Consider a solution of (1) consisting of an incident and a reflected contribution on the right and a transmitted one on the left,

$$\psi(x) = \begin{cases} A_i e^{-i\omega x} + A_r e^{+i\omega x} & , x \rightarrow +\infty, \\ A_t e^{-i\omega x} & , x \rightarrow -\infty. \end{cases} \quad (3)$$

From this, one can define the reflection and transmission coefficients  $R(\omega) = A_r/A_i$  and  $T(\omega) = A_t/A_i$  respectively, and one sees that the QNM frequencies determined by (2) are poles of the reflection coefficient [6].

Consider now the semi-open problem where a wall of reflectivity  $\varepsilon$  is situated at  $x_b$  such that  $V(x_b)$  is effectively zero. The boundary condition becomes,

$$\psi(x \rightarrow x_b) \propto \varepsilon e^{i\omega(x-x_b)} + e^{-i\omega(x-x_b)}. \quad (4)$$

We choose a constant  $\varepsilon \in [0, 1]$ , allowing us to vary the amount of absorption at the wall: for  $\varepsilon = 1$  the wall is fully reflective whilst for  $\varepsilon = 0$  we recover the open problem [38]. The compatibility of (4) with (3) implies the following resonance condition [39],

$$\varepsilon R(\omega) e^{2i\omega x_b} = 1. \quad (5)$$

The QNM condition is retrieved in the  $\varepsilon \rightarrow 0$  limit, whilst for a finite reflectivity one should expect the resonances to deviate from the ones of the open system. This is well understood in the context of spectral stability analysis, where a small perturbation of  $V$  can significantly modify the spectrum [17]. The continuous evolution of the resonances in the complex plane as  $\varepsilon$  increases can be described in terms of integral curves of an ordinary differential equation [40]. The resonance condition (5) can be expressed as  $\varepsilon - R^{-1}(\omega_n^\varepsilon) = 0$ , where  $\omega_n^\varepsilon$  are the resonant frequencies indexed by  $n = 0, 1, \dots$ , and the superscript indicates the value at a particular  $\varepsilon$ . By differentiating with respect to the reflectivity, one gets,

$$\frac{\partial \omega_n}{\partial \varepsilon} = - \frac{R^2}{R'} \Big|_{\omega=\omega_n} \equiv H(\omega_n), \quad (6)$$

where  $R' = \partial_\omega R$ . The right-hand side defines a vector field along which the real and imaginary parts of the resonances evolve as we change the boundary's reflectivity.

*Pöschl-Teller potential.*—We now apply this framework to the Pöschl-Teller (PT) potential,

$$V_{\text{pt}}(x) = \frac{V_0}{\cosh^2(\alpha x)}. \quad (7)$$

In this case, (1) has an analytical solutions in the form  $e^{-i\omega t}\psi(x)$ . Defining a new variable  $y = 1/(1 + e^{2\alpha x})$ , the spatial part can be written as,

$$\psi(y) = (1-y)^{-i\omega/2\alpha} \left[ A y^{-i\omega/2\alpha} {}_2F_1(a, b, c; y) + B y^{i\omega/2\alpha} {}_2F_1(1+a-c, 1+b-c, 2-c; y) \right], \quad (8)$$

where  $A, B$  are constants and  ${}_2F_1$  hypergeometric functions [41] whose parameters are given by,

$$a, b = \frac{1}{2} - i\omega/\alpha \pm \frac{1}{2} \sqrt{1 - \frac{4V_0}{\alpha^2}}, \quad c = 1 - i\omega/\alpha, \quad (9)$$

with the + (−) sign for  $a$  ( $b$ ). Without loss of generality, from now on we take  $V_0 = 1$ . To impose the resonance condition (5), we need to define the reflection coefficient. Assuming that  $V(x_b)$  is close to vanishing, (8) is well-approximated by its asymptotic expansion and the in- and out-going wave contributions can be identified (see Appendix B). Their ratio gives the reflection coefficient,

$$R = \frac{\Gamma(a)\Gamma(b)}{\Gamma(c-a)\Gamma(c-b)} \frac{\Gamma(i\omega/\alpha)}{\Gamma(-i\omega/\alpha)}. \quad (10)$$

Poles of this expression give the QNMs of the open system,

$$\omega_n^{\varepsilon=0} = \pm \sqrt{1 - \alpha^2/4} - i\alpha(2n+1)/2, \quad (11)$$

where  $n$  is called the overtone number. All QNM frequencies of the PT potential share the same real part and differ only in their imaginary part. The mode with  $n = 0$  is called the fundamental mode, since it has the longest lifetime, whereas overtones with  $n > 0$  are characterised by stronger damping [6]. This particular feature, also relevant for astrophysical black holes, renders the observation of overtones difficult. Consequently, the analysis of the systems' properties is often limited to the detection of the fundamental mode.

Resonances of the semi-open system are obtained by numerically solving (5). In Fig. 1a, we display their continuous migration in the complex plane as  $\varepsilon$  is varied. Large yellow dots represent QNMs of the open system for  $\varepsilon = 0$  and, as  $\varepsilon$  is increased, the resonances migrate down toward the real line. We can identify three qualitatively different types of QNM when  $\varepsilon = 1$ . Modes with  $\text{Re}[\omega] = 0$  correspond to purely damped solutions (discussed in [40]). Modes with  $0 < \text{Re}[\omega] < \tilde{\omega}_r$  are damped oscillatory modes which are localised between the hard wall and the barrier  $V$ . These are quasibound states (QBS) which need to tunnel through  $V$  to escape to  $x \rightarrow -\infty$ , leading to long lifetimes. Finally, modes with  $\text{Re}[\omega] > \tilde{\omega}_r$  pass over the barrier and experience only a small amount of reflection due to the inhomogeneous nature of  $V$ . Consequently, they are more strongly damped and can be identified with the new overtones of the system. These overtones possess distinctly different real frequencies and an imaginary part which is reduced significantly relative to the open system.

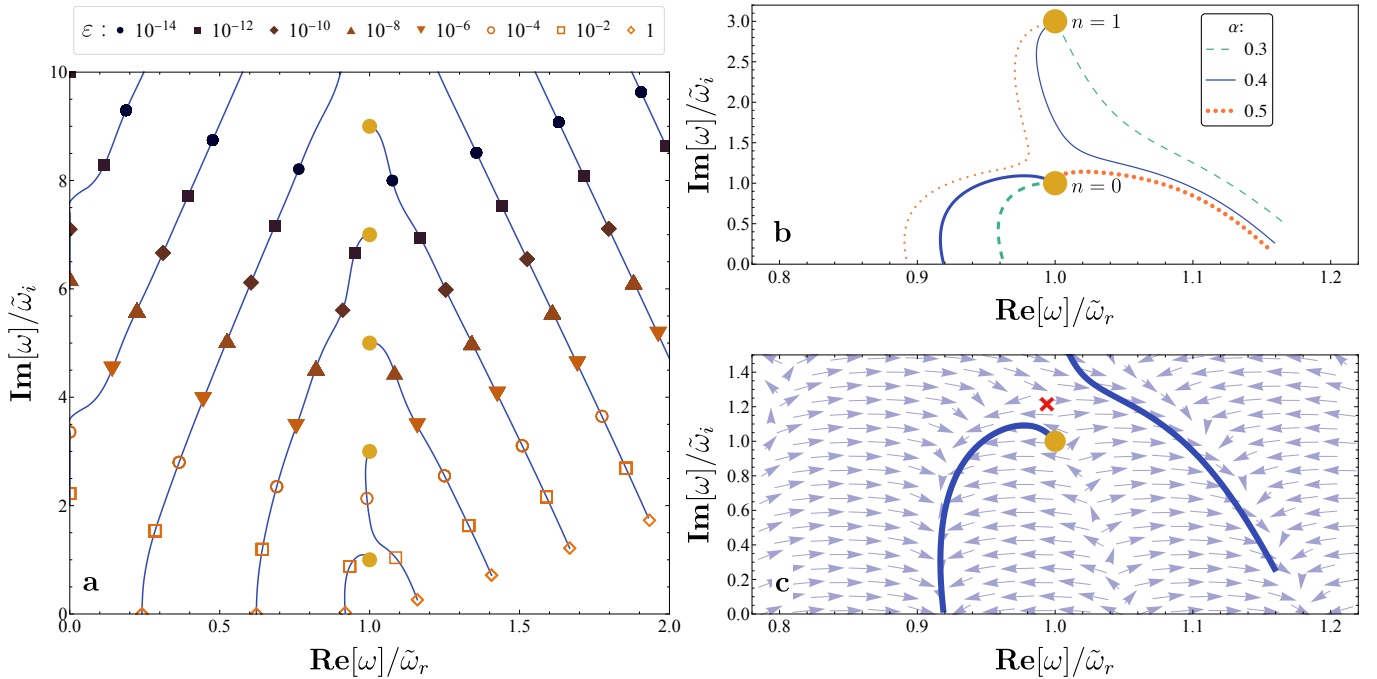


FIG. 1. **a.** Trajectories in the complex plane of the first 11 resonances of the PT potential with a partially-reflective barrier relative to the fundamental QNM  $\omega_{n=0}^{\varepsilon=0} \equiv \tilde{\omega}_r + i\tilde{\omega}_i$ . Here we take  $\alpha = 0.4$  and the position of the wall is fixed at  $x_b = 10$ . The large yellow dots represent QNMs of the open system, whereas the blue lines are obtained varying  $\varepsilon$ . Coloured markers label the resonances at particular values of reflectivity. **b.** Trajectories of the resonances as reflectivity increases, for  $\alpha = 0.5$  (Green, dashed),  $\alpha = 0.4$  (Blue, solid),  $\alpha = 0.3$  (Orange, dotted) and  $x_b = 10$ . The yellow dots are  $\omega_{n=0,1}^{\varepsilon=0}$  and the lines end at  $\varepsilon = 1$ . **c.** The migration of the resonance is compared against the vector field  $H(\omega)$  for  $\alpha = 0.4$ . The red cross is placed on the repelling point, i.e. the pole of  $H$ .

In Fig. 1b, we provide a closeup of the  $n = 0, 1$  modes and show the effect of changing  $\alpha$ , i.e. the width of the PT potential. As  $\alpha$  gets larger, the potential barrier becomes narrower and more QBSs can fit in the cavity formed by the hard wall and potential barrier. In the complex  $\omega$  plane, one would then see all the  $\omega_n^{\varepsilon=1}$  moving toward lower  $\text{Re}[\omega]$  and the trajectories emerging from  $\omega_n^{\varepsilon=0}$  orbiting around the yellow points in Fig. 1a in the clockwise direction. However, at critical values of  $\alpha$ , there can be discontinuous jumps where the migration lines ending at  $\omega_n^{\varepsilon=1}$  change which of the  $\omega_n^{\varepsilon=0}$  they are connected to. These discontinuous jumps are related to repelling points of (5), illustrated as the red cross in Fig. 1c. A migration line is an integral curve of the vector field  $H(\omega)$ , defined in (6), and is deflected either to the left or to the right of the repelling point, i.e. the poles of  $H(\omega)$ , as the resonances move down toward the real axis. A small change in  $\alpha$  can change the vector field such that a left-directed line suddenly changes to a right-directed line. This is exemplified by the transition from  $\alpha = 0.4$  to  $\alpha = 0.5$  on Fig. 1b where for  $\alpha = 0.4$ , the line emerging from  $\omega_{n=0}^{\varepsilon=0}$  ( $\omega_{n=1}^{\varepsilon=0}$ ) is directed left (right), but switches direction when increasing to  $\alpha = 0.5$ . Although the trajectories are discontinuous when varying  $\alpha$ , and similar behaviour would occur when varying  $x_b$ , what matters for us is that for  $\alpha$  and  $x_b$  fixed, varying  $\varepsilon$  defines a continuous map from the open system resonances to the QBS

and the new overtones of the semi-open system. Hence,  $\varepsilon$  is a dial which allows us to smoothly switch on this additional structure.

*Numerical simulations.*—A consequence of the reflective boundary is that the new overtones have distinct real frequencies and longer lifetimes, facilitating their detection. We demonstrate this via a numerical simulation. The wave equation (1) is simulated using a method of lines algorithm (details in Appendix A). In Fig. 2, a Gaussian pulse is evolved toward the barrier from the side of the open boundary. We illustrate the response signal, in both the time and frequency domains (left and right panels respectively) after the initial pulse has passed for various  $\varepsilon$ , i.e. as the boundary is made more reflective, focusing on values which make the decay times of  $n = 0, 1$  comparable (see Fig. 1). For the open system, we observe the characteristic QNM waveform, corresponding to a singly peaked frequency spectrum. However, for semi-open systems, the signal becomes more complicated, characterised by interference between multiple frequencies in the time domain which correspond to more than one peak in Fourier space. Notably, the peak corresponding to  $\omega_{n=0}^{\varepsilon=0}$  splits in two, the left peak corresponding to the highest frequency QBS and the right peak to the first of the new overtones. For a partially absorbing wall, we observe that this overtone is actually the dominant signal when we measure near the open boundary. When the

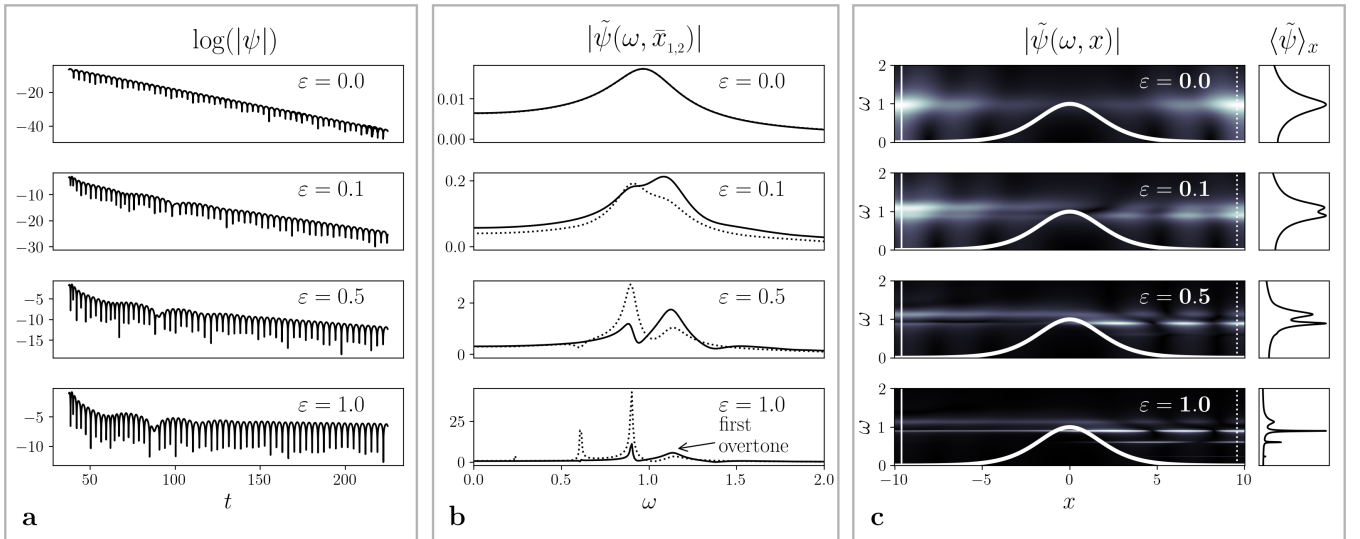


FIG. 2. **a.** Ringdown signal in time and frequency domain for the same  $x_b$  and  $\alpha$  in Fig. 1a. The logarithm of the absolute value of the signal close to the reflective wall is shown on the left panels. For the open-system  $\varepsilon = 0$ , we observe the characteristic QNM response whilst for  $\varepsilon \neq 0$ , the signal is characterised by a fast (slowly) decaying signal at early (late) times. **b.** We show Fourier transform of the signal at  $\bar{x}_1$  near the wall (dotted line) and on the open side of the system at  $\bar{x}_2$  (solid). The first overtone (the peak to the right of  $\text{Re}[\omega] > 1$ ) becomes more pronounced for larger  $\varepsilon$  since the damping is reduced relative to  $\varepsilon = 0$ , and corresponds to the short-lived part of the time domain signal. **c.** We plot the Fourier transform of the signal at each point to illustrate the spatial features for the resonant modes against the PT potential (thick white line). The signal is normalised such that the colour bar goes from 0 (black) to 1 (white). The dotted and the solid lines label  $\bar{x}_1$  and  $\bar{x}_2$  respectively. The spectrum averaged over the  $x$  axis is showed on the right side.

wall is fully reflective, the dominant signal comes from the QBS due to their long lifetimes, although our simulations suggest that the first overtone is still detectable. In Fig. 2c, we illustrate the full spatial waveform as a function of frequency, illustrating how the different resonant modes (indicated by bright horizontal lines) are bound by the potential barrier. As expected, modes scattering with the wider part of the barrier experience less leakage. Note that although format in Fig. 2a will be familiar to gravitational community, the equivalent representations in panels b and c emerge naturally in the data analysis of analogue experiments [35, 42] and carry more information about the spatial profile of the modes.

Although Gaussian pulses are frequently used in numerical studies to stimulate the system [6], a more natural perturbing mechanism from the experimental perspective is broadband mechanical noise [35, 36]. In Fig. 3, we take  $\Psi(x, t = 0) = 0$  as initial condition but generate random noise on the side of the open boundary at each time step for the duration of the simulation. We then Fourier transform the signal after the noise has propagated across the system and take the average on the side of the barrier near the wall. We collect statistics over 500 iterations and display the mean and the variance. In the open system, there is no distinct signal; at high frequency we observe the noise level and at lower frequencies a suppression due to the presence of the barrier. For partial absorption, we observe a series of peaks emerging above the noise level, which become very pronounced for

the fully reflective wall. Notably, the first overtone appears as a distinct signal in the data, suggesting that the combination of a finite size system with mechanical noise may be sufficient ingredients to detect QNM overtones in analogue experiments. This method of resonant stimulation is akin to that of the driven, damped harmonic oscillator, where the energy input from the driving force is balanced by the energy loss due to dissipation (in our case resulting from the open boundary).

*Discussion.*—Finite-size constraints of analogue experiments might initially appear as an obstacle to simulating black hole ringdown - a phenomenon typically associated with open (i.e. spatially unbounded) systems. Counter to this expectation, our results demonstrate that the introduction of such confining mechanisms, in fact, becomes a valuable tool for studying the quasinormal modes (QNMs) and the role of the overtones in shaping the ringdown signal. The set-up we have presented (based on a Poschl-Teller potential) captures the essential physics of experimentally realisable black hole analogues, where the partially reflective boundary models the experimental confinement and the open boundary represents the analogue black hole horizon. As the reflectivity of the closed boundary is increased from zero, the QNMs of the open system migrate continuously along trajectories in the complex frequency plane toward the real axis. In addition to the familiar quasibound states of semi-open systems, the modified spectrum contains a hierarchy of overtones with distinct oscillation frequencies and sub-

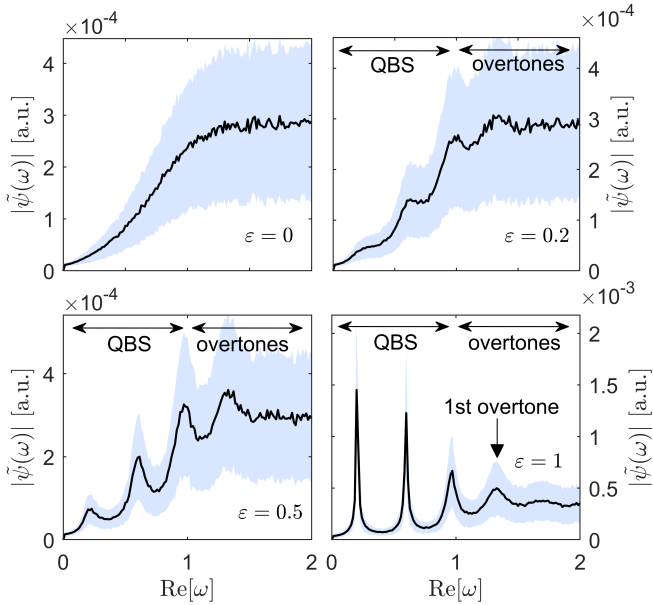


FIG. 3. The systems response in the frequency domain when stimulated with mechanical noise. We take the average over 500 runs (black lines) and display the standard deviation as the shaded regions. The semi-open system is characterised by the presence of well defined resonance peaks. In particular, we manage to resolve the first overtone above the noise level. The data is for a potential with  $\alpha = 1$  and a wall at  $x_b = 10$ .

stantially longer lifetimes compared to the open system.

These two features significantly increase the prospect of a detecting QNM overtones in an analogue experiment, as exemplified by our numerical simulations. An added consequence is that the frequency response of the semi-open system to a random driving signal is sharply peaked around the QNMs, a feature which is absent in the open system as it relies on constructive interference with reflected waves. A measurement of such a signal could prove particularly natural for experiments where noise (e.g. thermal or mechanical) is always present. Indeed, this mechanism may be responsible for the QNM oscillations measured in [37].

From a gravity perspective, the semi-open problem has been addressed in the context of neutron stars/compact objects and anti-de Sitter spacetimes. The focus (in the

case of the former) is usually on the new bound states that arise in the spectrum, and (in the latter) on echoes of the usual QNM response. In our case, where the reflecting boundary is close to the peak of the scattering potential, we have shown that the new overtones are a prominent feature of linear response, and that random noise is a viable probe of the spectrum. In addition to the aforementioned astrophysical settings, stimulating QNMs in this fashion may also be relevant for a black hole surrounded by matter [9, 43, 44] or hypothetical ultra-light fields [45, 46].

Furthermore, discerning the roles of nonlinearities and overtones in shaping the ringdown waveform is a central topic of research in the gravitational wave community [47, 48]. Understanding the interplay of these two competing effects is therefore desirable. Finite size black hole simulators may be useful in this regard, since both the nonlinearities and overtone lifetimes can be experimentally controlled (the former through signal amplitudes and the latter using the boundary reflectivity). This feature stands out as an enhanced capability of semi-open systems compared with gravitational black holes which radiate to infinity, where a consequence of the no-hair theorem is that the overtone lifetime is not an adjustable parameter [6].

*Acknowledgements.*—L.S. and S.P. would like to thank Théo Torres for providing valuable insight on spectral stability based on unpublished work with Sam Dolan. We are grateful to Patrik Švančara, Pietro Smaniotto and Thomas Sotiriou for helpful discussions and comments on the manuscript. We also thank Paolo Pani for feedback. L.S. and S.W. gratefully acknowledge the support of the Leverhulme Research Leadership Award (RL-2019-020). S.P., R.G. and S.W. extend their appreciation to the Science and Technology Facilities Council for their generous support in Quantum Simulators for Fundamental Physics (QSimFP), (ST/T005858/1 and ST/T006900/1), as part of the UKRI Quantum Technologies for Fundamental Physics program. S.W. also acknowledges the Royal Society University Research Fellowship (UF120112). R.G. acknowledges support from the Perimeter Institute. Research at Perimeter Institute is supported by the Government of Canada through the Department of Innovation, Science and Economic Development Canada and by the Province of Ontario through the Ministry of Research, Innovation and Science.

[1] B. P. Abbott *et al.*, Observation of gravitational waves from a binary black hole merger, *Phys. Rev. Lett.* **116**, 061102 (2016).  
[2] V. Ferrari and B. Mashhoon, New approach to the quasi-normal modes of a black hole, *Physical Review D* **30**, 295 (1984).  
[3] F. Echeverria, Gravitational-wave measurements of the mass and angular momentum of a black hole, *Phys. Rev. D* **40**, 3194 (1989).

[4] K. D. Kokkotas and B. G. Schmidt, Quasi-normal modes of stars and black holes, *Living Reviews in Relativity* **2**, 1 (1999).  
[5] V. Cardoso, A. S. Miranda, E. Berti, H. Witek, and V. T. Zanchin, Geodesic stability, lyapunov exponents, and quasinormal modes, *Phys. Rev. D* **79**, 064016 (2009).  
[6] E. Berti, V. Cardoso, and A. O. Starinets, Quasinormal modes of black holes and black branes, *Classical and Quantum Gravity* **26**, 10.1088/0264-9381/26/16/163001

- (2009).
- [7] P. Amaro-Seoane, H. Audley, S. Babak, J. Baker, E. Barausse, P. Bender, E. Berti, P. Binetruy, M. Born, D. Boroluzzi, *et al.*, Laser interferometer space antenna, arXiv preprint arXiv:1702.00786 (2017).
- [8] M. Maggiore, C. Van Den Broeck, N. Bartolo, E. Belgacem, D. Bertacca, M. A. Bizouard, M. Branchesi, S. Clesse, S. Foffa, J. García-Bellido, *et al.*, Science case for the Einstein telescope, *J. Cosmo. Astro Phys.* **2020**, 050 (2020).
- [9] E. Cannizzaro, T. F. Spieksma, V. Cardoso, and T. Ikeda, The impact of plasma on the relaxation of black holes, arXiv preprint arXiv:2405.05315 (2024).
- [10] M. H.-Y. Cheung, V. Baibhav, E. Berti, V. Cardoso, G. Carullo, R. Cotesta, W. Del Pozzo, F. Duque, T. Helfer, E. Shukla, and K. W. K. Wong, Nonlinear effects in black hole ringdown, *Phys. Rev. Lett.* **130**, 081401 (2023).
- [11] H.-P. Nollert, About the significance of quasinormal modes of black holes, *Phys. Rev. D* **53**, 4397 (1996).
- [12] J. Aguirregabiria and C. Vishveshwara, Scattering by black holes: a simulated potential approach, *Physics Letters A* **210**, 251 (1996).
- [13] H.-P. Nollert and R. H. Price, Quantifying excitations of quasinormal mode systems, *Journal of Mathematical Physics* **40**, 980 (1999).
- [14] M. H.-Y. Cheung, K. Destounis, R. P. Macedo, E. Berti, and V. Cardoso, Destabilizing the fundamental mode of black holes: The elephant and the flea, *Phys. Rev. Lett.* **128**, 111103 (2022).
- [15] H. Witek, V. Cardoso, A. Ishibashi, and U. Sperhake, Superradiant instabilities in astrophysical systems, *Phys. Rev. D* **87**, 043513 (2013).
- [16] Y. Huang and H. Zhang, Quasibound states of charged dilatonic black holes, *Phys. Rev. D* **103**, 044062 (2021).
- [17] J. L. Jaramillo, R. P. Macedo, and L. A. Sheikh, Pseudospectrum and black hole quasinormal mode instability, *Phys. Rev. X* **11**, 031003 (2021).
- [18] J. L. Jaramillo, R. P. Macedo, and L. A. Sheikh, Gravitational wave signatures of black hole quasinormal mode instability, *Phys. Rev. Lett.* **128**, 211102 (2022).
- [19] E. Maggio, P. Pani, and V. Ferrari, Exotic compact objects and how to quench their ergoregion instability, *Phys. Rev. D* **96**, 104047 (2017).
- [20] A. Testa and P. Pani, Analytical template for gravitational-wave echoes: Signal characterization and prospects of detection with current and future interferometers, *Phys. Rev. D* **98**, 044018 (2018).
- [21] E. Maggio, V. Cardoso, S. R. Dolan, and P. Pani, Ergoregion instability of exotic compact objects: Electromagnetic and gravitational perturbations and the role of absorption, *Phys. Rev. D* **99**, 064007 (2019).
- [22] E. Maggio, L. Buoninfante, A. Mazumdar, and P. Pani, How does a dark compact object ringdown?, *Phys. Rev. D* **102**, 064053 (2020).
- [23] L.-P. Euvé, F. Michel, R. Parentani, T. G. Philbin, and G. Rousseaux, Observation of noise correlated by the Hawking effect in a water tank, *Phys. Rev. Lett.* **117**, 121301 (2016).
- [24] J. Steinhauer, Observation of self-amplifying Hawking radiation in an analogue black-hole laser, *Nat. Phys.* **10**, 864 (2014).
- [25] J. Steinhauer, Observation of quantum Hawking radiation and its entanglement in an analogue black hole, *Nat. Phys.* **12**, 959–965 (2016).
- [26] S. Weinfurtner, E. W. Tedford, M. C. J. Penrice, W. G. Unruh, and G. A. Lawrence, Measurement of stimulated Hawking emission in an analogue system, *Phys. Rev. Lett.* **106**, 021302 (2011).
- [27] M. Visser and S. Weinfurtner, Vortex analogue for the equatorial geometry of the Kerr black hole, *Class. Quantum Gravity* **22**, 2493 (2005).
- [28] T. Torres, S. Patrick, A. Coutant, M. Richartz, E. W. Tedford, and S. Weinfurtner, Rotational superradiant scattering in a vortex flow, *Nature Physics* **13**, 10.1038/nphys4151 (2017).
- [29] D. D. Solnyshkov, C. Leblanc, S. V. Koniakhin, O. Bleu, and G. Malpuech, Quantum analogue of a Kerr black hole and the Penrose effect in a Bose-Einstein condensate, *Phys. Rev. B* **99**, 214511 (2019).
- [30] M. C. Braidotti, R. Prizia, C. Maitland, F. Marino, A. Prain, I. Starshynov, N. Westerberg, E. M. Wright, and D. Faccio, Measurement of Penrose superradiance in a photon superfluid, *Phys. Rev. Lett.* **128**, 013901 (2022).
- [31] M. Cromb, G. M. Gibson, E. Toninelli, M. J. Padgett, E. M. Wright, and D. Faccio, Amplification of waves from a rotating body, *Nat. Phys.* **16**, 1069 (2020).
- [32] M. J. Jacquet, L. Giacomelli, Q. Valnais, M. Joly, F. Claude, E. Giacobino, Q. Glorieux, I. Carusotto, and A. Bramati, Quantum vacuum excitation of a quasinormal mode in an analog model of black hole spacetime, *Phys. Rev. Lett.* **130**, 111501 (2023).
- [33] C. Burgess, S. Patrick, T. Torres, R. Gregory, and F. König, Quasinormal modes of optical solitons, *Phys. Rev. Lett.* **132**, 053802 (2024).
- [34] S. Patrick, A. Coutant, M. Richartz, and S. Weinfurtner, Black hole quasibound states from a draining bathtub vortex flow, *Physical Review Letters* **121**, 10.1103/PhysRevLett.121.061101 (2018).
- [35] T. Torres, S. Patrick, M. Richartz, and S. Weinfurtner, Quasinormal mode oscillations in an analogue black hole experiment, *Physical Review Letters* **125**, 10.1103/PhysRevLett.125.011301 (2020).
- [36] P. Švančara, P. Smaniotto, L. Solidoro, J. F. MacDonald, S. Patrick, R. Gregory, C. F. Barenghi, and S. Weinfurtner, Rotating curved spacetime signatures from a giant quantum vortex, *Nature* **628**, 66 (2024).
- [37] T. Torres, S. Patrick, and R. Gregory, Imperfect draining vortex as analog extreme compact object, *Phys. Rev. D* **106**, 045026 (2022).
- [38] Note that our choice of  $\varepsilon$  real and positive corresponds to a Neumann boundary condition in the case of a complete reflection, whereas choosing  $\varepsilon$  negative/complex would lead to a Dirichlet/Robin boundary condition. In general,  $\varepsilon$  could depend on  $\omega$  but for the sake of simplicity, we model it here as a constant.
- [39] C. F. B. Macedo, T. Stratton, S. Dolan, and L. C. B. Crispino, Spectral lines of extreme compact objects, *Phys. Rev. D* **98**, 104034 (2018).
- [40] S. Dolan and T. Torres, Spectral (in)stability of black holes under potential perturbations, work in progress.
- [41] J. J. Florentin, M. Abramowitz, and I. A. Stegun, Handbook of mathematical functions., *The American Mathematical Monthly* **73**, 10.2307/2314682 (1966).
- [42] P. Švančara, P. Smaniotto, L. Solidoro, J. F. MacDonald, S. Patrick, R. Gregory, C. F. Barenghi, and S. Weinfurtner, Rotating curved spacetime signatures from a giant quantum vortex, *Nature* , 1 (2024).

- [43] E. Barausse, V. Cardoso, and P. Pani, Can environmental effects spoil precision gravitational-wave astrophysics?, *Phys. Rev. D* **89**, 104059 (2014).
- [44] P. S. Cole, G. Bertone, A. Coogan, D. Gaggero, T. Karydas, B. J. Kavanagh, T. F. M. Spieksma, and G. M. Tomaselli, Distinguishing environmental effects on binary black hole gravitational waveforms, *Nat. Astro.* **7**, 943 (2023).
- [45] O. A. Hannuksela, K. W. K. Wong, R. Brito, E. Berti, and T. G. F. Li, Probing the existence of ultralight bosons with a single gravitational-wave measurement, *Nat. Astro.* **3**, 447 (2019).
- [46] D. Baumann, G. Bertone, J. Stout, and G. M. Tomaselli, Sharp signals of boson clouds in black hole binary inspirals, *Phys. Rev. Lett.* **128**, 221102 (2022).
- [47] L. London, D. Shoemaker, and J. Healy, Modeling ring-down: Beyond the fundamental quasinormal modes, *Phys. Rev. D* **90**, 124032 (2014).
- [48] K. Mitman, M. Lagos, L. C. Stein, S. Ma, L. Hui, Y. Chen, N. Deppe, F. Hébert, L. E. Kidder, J. Moxon, *et al.*, Nonlinearities in black hole ringdowns, *Phys. Rev. Lett.* **130**, 081402 (2023).

### Appendix A: Numerical simulations

We simulate (1) using the method of lines. First we define a spatial grid  $x_k$  with  $k = 1 \dots N$  and  $h = x_{k+1} - x_k$  and a 3-point centred difference stencil for the second derivative,

$$\partial_x^2 \Psi_k = \frac{\Psi_{k+1} - 2\Psi_k + \Psi_{k-1}}{h^2}. \quad (1)$$

We then define  $\Pi = \partial_t \Psi$  and cast (1) in the form,

$$\partial_t \begin{pmatrix} \Psi \\ \Pi \end{pmatrix} = \begin{pmatrix} 0 & 1 \\ \partial_x^2 - V & 0 \end{pmatrix} \begin{pmatrix} \Psi \\ \Pi \end{pmatrix}, \quad (2)$$

and use a fourth-order Runge-Kutta algorithm to update the field at the next time step. This method allows us to implement absorbing boundary conditions in a simple way. At the edge of the domain where  $V \simeq 0$  our solution will be either a left-moving or right-moving plane wave, whose derivatives satisfy  $\partial_x \Psi = \pm \partial_t \Psi$ . At the same order of accuracy in  $h$ , the 3-point centred difference stencil for the first derivative,

$$\partial_x \Psi_k = \frac{\Psi_{k+1} - \Psi_{k-1}}{2h}, \quad (3)$$

gives  $\Psi_0 = \Psi_2 - 2h\Pi_1$  at the left boundary and  $\Psi_{N+1} = \Psi_{N-1} - 2h\Pi_N$  at the right boundary. Hence, we modify our stencil for  $\partial_x^2$  on the boundaries,

$$\partial_x^2 \Psi_1 = \frac{2\Psi_2 - 2\Psi_{k-1}}{h^2} - \frac{2\Pi_1}{h}. \quad (4)$$

and similarly for the point  $k = N$ . Note that without the term proportional to  $\Pi_1$ , this would just be the second derivative implemented with Neumann boundary conditions, say  ${}^N\partial_x^2$ . Our numerical equation of motion then gets modified to,

$$\partial_t \begin{pmatrix} \Psi \\ \Pi \end{pmatrix} = \begin{pmatrix} \mathbf{0} & \mathbf{I} \\ {}^N\partial_x^2 - V & B \end{pmatrix} \begin{pmatrix} \Psi \\ \Pi \end{pmatrix}, \quad (5)$$

where  $B = -(2/h)\text{diag}(\mu, 0, \dots, 0, 1)$  is a diagonal matrix with non-zero entries in the top-left and bottom-right corner. The parameter  $\mu$  allows us to tune between a fully reflective Neumann boundary condition on one side for  $\mu = 0$  and a completely open boundary for  $\mu = 1$ . The relation between  $\mu$  and the reflectivity  $\varepsilon$  used in the main text is,

$$\mu = \frac{1 - \varepsilon}{1 + \varepsilon}. \quad (6)$$

### Appendix B: Pöschl-Teller resonance condition

The linear wave equation (1) with the Pöschl-Teller potential reads:

$$\frac{\partial^2 \psi}{\partial x^2} - \left( \omega^2 - \frac{V_0}{\cosh(\alpha x)^2} \right) \psi = 0. \quad (1)$$

The equation can be reduced to an hypergeometric differential equation [41]:

$$(1-y)y \frac{\partial^2 \phi}{\partial y^2} + [c - (a+b+1)y] \frac{\partial \phi}{\partial y} - ab\phi = 0, \quad (2)$$

whose solution is (8), by introducing the variable:

$$\phi = \psi((1-y)y)^{i\omega/2\alpha}.$$

The parameters  $a, b, c$  and the spatial variable  $y$  are given in the main text. In order to impose the radiating boundary condition (2) at  $x \rightarrow -\infty$ , one sees that for large negative positions  $y^{\pm i\omega/2\alpha} \rightarrow e^{\pm i\omega x}$ . Hence, it is possible to identify the right-moving contribution in (8) and then to impose the boundary condition on the left with  $B = 0$ .

To look at the behaviour of the solution as  $x \rightarrow +\infty$ , i.e.  $y \rightarrow 1$ , one can use the transformation rule of the hypergeometric functions [41] to get

$$\psi = Ay^{-i\omega/2\alpha} \left[ (1-y)^{i\omega/2\alpha} \frac{\Gamma(c)\Gamma(a+b-c)}{\Gamma(a)\Gamma(b)} {}_2F_1(c-a, c-b, c^*, 1-y) + (1-y)^{-i\omega/2\alpha} \frac{\Gamma(c)\Gamma(c-a-b)}{\Gamma(c-a)\Gamma(c-b)} {}_2F_1(a, b, c, 1-y) \right],$$

We can identify the out-going and in-going contributions as  $x \rightarrow \infty$  by noticing that

$$(1 - y)^{\pm i\omega/2\alpha} \xrightarrow{x \gg 1} e^{\mp i\omega x}.$$

Therefore, one can define a Reflection Coefficient for the PT potential as the ratio between the out-going and in-going contribution at the right of the potential, resulting in (10)